Aerodynamic analysis of a novel pitch control strategy and parameter combination for vertical axis wind turbines

Qiang Zhang [a], Musa Bashir [c], Weipao Miao [a], Qingsong Liu [a], Chun Li[a,b,*], Minnan Yue[a], Peilin Wang[a],

a. School of Energy and Power Engineering, University of Shanghai for Science and Technology, Shanghai, 200093. China

b. Shanghai Key Laboratory of Multiphase Flow and Heat Transfer in Power Engineering, Shanghai, 200093. China

c Liverpool Logistics, Offshore and Marine (LOOM) Research Institute, Liverpool John Moores University, Liverpool, Byrom Street, L3 3AF, UK

Abstract

The performance of a vertical axis wind turbine (VAWT) deteriorates at low tip speed ratios (TSR) and it is mainly characterized by flow separation and dynamic stall. Several mitigating techniques have been developed recently based on flow separation and dynamic stall research activities. One of such techniques is the use of blade pitch angle control, which shows very promising optimal performance in VAWTs. However, its adaptation for periodic variation of the angle of attack remains an important issue that needs to be addressed urgently. Therefore, this paper proposes a novel pitch control strategy based on the VAWT-shape pitch motion to achieve blade dynamic pitch with the rotational parameters (TSR and azimuth angle). The pitch scale factor (μ) is introduced to proportionally vary the angle of attack. High accuracy computational fluid dynamics (CFD) methods are used to simulate dynamic changes in pitch angle, flow field and vortex shedding vorticity, with the turbulence modelled using the SST k-ω model. The results show that a 146% increase in power coefficient can be achieved using a μ of 0.3 at TSR of 1.25. Additionally, the use of dual pitch scale factors (*dpsf*) in the windward and leeward regions causes intense transient torque fluctuations at 0° (360°) and 180° azimuths due to a breaking distance in pitch angular velocity at these azimuths. Adding a weight function into the fitting process of the *dpsf* pitch curve effectively minimize these fluctuations.

Keywords: Vertical axis wind turbines; Pitch control strategy; Pitch angular velocity; Aerodynamic analysis

Graphical Abstract

* Corresponding author: Chun Li. Tel: 86 19821232017. E-mail address: lichun_usst@163.com

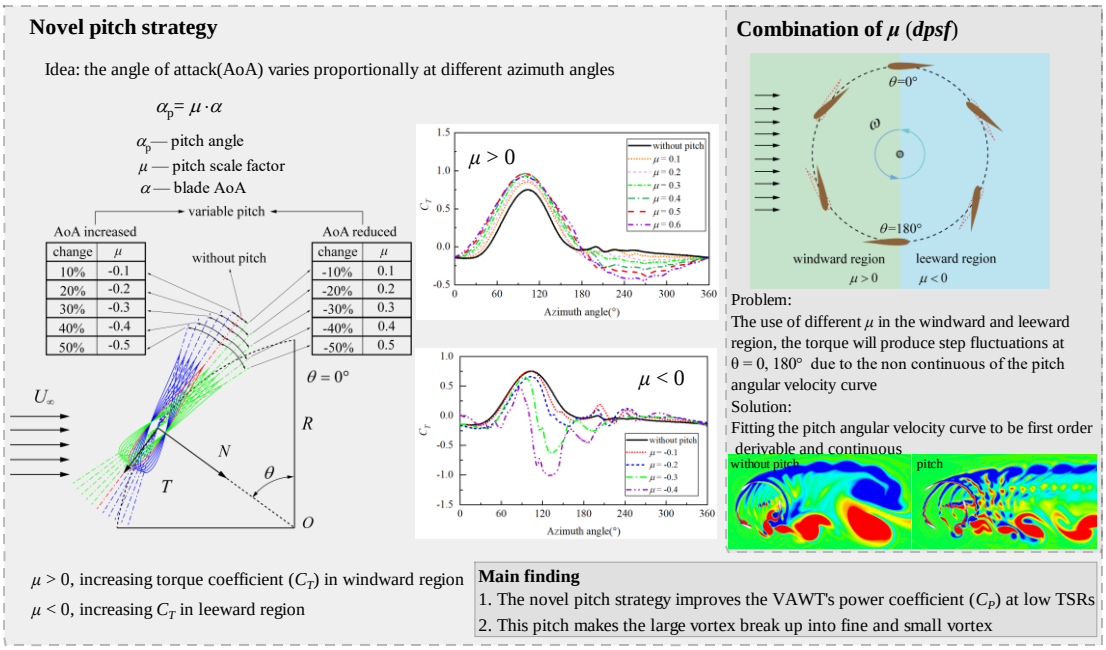

Nomenclature

2-D	Two-dimensional	α	Angle of Attack
3-D	Three-dimensional	α_p	Pitch angle
AoA	Angle of Attack	β	The angle of attack after pitch
CFD	Computational Fluid Dynamics	c	Chord length
psf	pitch scale factor	ω	Rotational speed of the rotor
dpsf	dual pitch scale factors	$\dot{\alpha}$	Blade rotation angular velocity
TSR	tip speed ratio	$\dot{\alpha}_p$	Blade pitch angular velocity
URANS	Unsteady Reynolds Averaged Navier Stokes	θ	Azimuthal angle
VAWT	vertical axis wind turbines	μ	Pitch scale factor
F_L	Lift	V	Blade speed
F_D	Drag	W	Relative wind speed
C_L	Lift coefficient	U	Wind speed
C_D	Drag coefficient	U_∞	The incoming wind speed
C_T	Torque coefficient	T	Torque
C_P	Power coefficient	ρ	Air density
$\Delta\theta$	Rotation angle per time step	$\Delta\varepsilon_{g+1,g}$	Difference in two power coefficient
Δt	Time step	$\Delta e_{g+1,g}$	Relative error of power coefficient
A	Wind wheel swept area	λ	Tip speed ratio
N_E	Number of elements	ΔI	Interface element size of rotation region
N_N	Number of nodes on airfoil profile	ΔI_B	Interface element size of blade region
N_{VAWT}	Number of blades	H	Height of blade
D	VAWT diameter of wind wheel	γ	Setting angle
D_r	Diameter of rotor	σ	Blade solidity
Re	Reynolds number	t	Physical time
Y^+	Dimensionless wall distance		

1. Introduction

The exploitation of renewable wind energy resources, which exists in abundance, has attracted strong interest [1]. There are two main types of fluid machines that convert wind kinetic energy into electrical power, namely, horizontal axis wind turbines (HAWTs) and vertical axis wind turbines (VAWTs) [2]. Compared with HAWTs, VAWTs have advantages such as easy installation and maintenance, low manufacturing cost, omni-wind direction, lower center of mass and the generator not constrained on top of the tower [3,4,5]. However, the low power output of VAWTs limits their development [6,7]. For VAWTs to take a substantial share in global wind energy production, it is particularly important to optimize its aerodynamic performance. To achieve this goal, improvements are generally required in blade profile [8,9], number of blades [10], blade solidity [11], morphing blades [12], free-flow turbulence intensity [13], and pitch angle [14,15].

The angle of attack (AoA) is an important factor affecting the aerodynamic performance of VAWT blades. Excessive AoA can deteriorate the aerodynamic performance of VAWT. A direct solution to this problem is to reduce the AoA by controlling the pitch in order to improve the self-starting capability and power output of VAWTs [16,17,18]. Kosaku et al [19] proposed the idea of controlling the AoA for VAWT blades to improve its aerodynamic performance, and this concept has started gaining traction in recent years.

In general, pitch techniques are classified as either passive or active [20]. The passive type is termed “pre-pitch”, in which the pitch angle is fixed and the blades do not perform pitch motion during rotation. Chen et al [21] and Bianchini et al [22] found that a suitable fixed pitch angle can improve the aerodynamic performance of VAWTs, especially for high solidity structure. Thumthae et al [23] obtained the fixed pitch angle that produces the maximum VAWT power coefficient at four blade tip speed ratios (TSR). The optimal pitch angles were 4.12°, 5.28°, 6.66°, and 8.76° for wind speeds of 7.2, 8.0, 9.0, and 10.5 m/s, respectively. Chen et al [24] configured a twin H VAWT located in the upwind and downwind regions. By studying 49 fixed pitch angles from -6° to 0°, the power coefficients of the two VAWTs were increased by 4.79% and 7.04%, respectively. Mazarbhuiya et al [25] studied the pitch of an asymmetric blade for VAWT at low wind speed. It was noted that a positive pitch angle (+5°) is beneficial to improving the performance of VAWT in the upwind region, while a negative pitch angle (-5°) in the downwind region provides better control of flow separation. Ardaneh et al [26] analyzed five different fixed pitch angles of the VAWT by two-dimensional (2-D) simulations, and then performed three-dimensional (3-D) simulations using the optimal pitch angle. The results show that a pitch angle of -2° improves the VAWT torque coefficient by 13.65% at TSR of 0.79. MacPhee et al [27] used elastic deformation to achieve passive pitch of the blade, which resulted in a 4.2% increase in the average lift-to-drag ratio for monitoring the AoA. Maeda et al [28] studied the flow characteristics of VAWT by using wind tunnel and field experiments, and the measured data found that the power coefficient was maximum at a blade pitch angle of 6°. Huang et al [29] found that positively pitched blades (+10°) exhibit the greatest wake deflection, resulting in the highest annual power for a hypothetical downwind turbine aligned with the upwind turbine. Although the passive pitch can improve the self-starting torque and aerodynamic performance of the VAWT, the experimental results show that the maximum power coefficient is less than one-third of the theoretically calculated value [30].

Active pitch functions as a continuous variation of the pitch angle by means of a pushrod, cam or motor [31]. The variable pitch angle adjustment is more flexible and creates more room for VAWT performance improvement. Guo et al [32] compared the effects of fixed and variable pitch angle on

VAWT aerodynamic performance and found that the common variable pitch angle control strategy performs better than the optimal fixed pitch angle. Abdalrahman et al [33] studied the variable pitch angle strategy for different TSRs, using a combination of several fixed pitch angles at different azimuths and with limited enhancement of the VAWT power coefficient. However, Leblanc et al [34,35] measured the effects of pitch on the normal loads in each azimuth angle through experiment. The results show that changing the pitch angle excites a greater load in blade rotation. This is due to the greatly increased stall behavior of the VAWT at fixed pitch offsets. Therefore, finding a continuous variable pitch angle strategy is the key to achieving optimal active pitch control. However, due to the periodicity of the blade AoA, any variable pitch strategy must be periodic [36]. Paraschivoiu et al [37] developed an optimization tool for the variation of blade pitch angle for H-Darrieus 7kw VAWT. The pitch equation is formulated as a polynomial combination of sinusoidal curves. By optimizing the pitch variation within the low wind region, the annual power production of the VAWT can be enhanced by almost 30%. Jain et al [38] found that the amplitude of sinusoidal pitch must vary with TSR and higher amplitude at TSR less than 0.5 (approximately equal to 35°). The amplitude should not exceed 10° for TSR greater than 2.

Zhao et al [39] varied the AoA around 0° and 180° azimuths to improve the performance in these two negative torque regions, which resulted in an 18.9% increase in the power coefficient. Li et al [40] used a genetic algorithm to optimize five pitch strategy parameters with the objective of maximizing the power coefficient and smoothened the pitch curve using a third-order spline curve, which improved the power coefficient by 0.487 at a TSR of 4.94. However, this optimization method takes 145 hours to calculate the optimal pitch angle, which costs significant computational resources in practical applications. Chen et al [41] developed a control system with real-time feedback for blade pitch angle based on the flow velocity around the blade. Adjusting the blade AoA according to the optimal pitch angle at this stage improved the power coefficient by 12.7% at high TSR. However, the variation of wind speed leads to irregular pitch curve as well as transient torque fluctuations. Guevara et al [42] calculated the pitch angle corresponding to the maximum torque at each azimuth of the VAWT and active pitch according to this pitch angle, and the results showed a 13% increase in maximum power output. Zhang et al [43] found the optimal AoA for windward and leeward regions as 17.7° and -18.4°, respectively. The authors used the pitching technique to adjust the AoA, and the power coefficient was improved by 14.56% after fitting the pitching curve.

A favorable variable pitch angle strategy is fundamental to improving VAWT performance and requires the following characteristics:

1. A large pitch angle to reduce the AoA at low TSR to improve the wind energy utilization of the VAWT. Conversely, a small pitch angle is required to provide significant effects at high TSR [44].

2. During blade rotation, a large pitch angle at azimuths with large AoA is required to reduce AOA and to suppress flow separation, thus, enhancing the blade aerodynamic performance. Meanwhile, a small pitch angle at azimuths with small AoA is required to ensure good aerodynamic performance.

Matching the VAWT rotation parameters (TSR and azimuth angle) with the pitch angle can produce a positive effect that can enhance the blade aerodynamic performance. This is a very important issue in the study of blade pitch technology as it deals with how the pitch angle varies with the TSR and azimuth angle to improve the wind energy utilization of VAWTs.

In recent years, there have been several studies on the optimal pitch angle based on the real-

time feedback flow-field data from the external environment to control the pitch angle variation. In fact, the accuracy of the control system is noted to have a great impact on the effect of pitch control due to fast rotation speed of the VAWT. Maintaining the response speed makes the control system complex [45]. Therefore, a suitable and operable pitch angle control strategy is needed to overcome this complexity.

In view of the above shortcomings, research on active pitch technology is needed. Consequently, the motivation of this study is to propose a pitch control strategy to improve the wind energy utilization of VAWT based on the following aspects:

(a) pitch angle that continuously varies under different azimuth angles and cannot be simply combined with several fixed pitch angles.

(b) effects of azimuth and TSR on the pitch angle that can be considered at the same time. The relationship between the VAWT rotation parameters (TSR and azimuth angle) of rotation and the pitch control strategy needs to be established.

(c) Application of different pitch curves in the windward and leeward regions due to the different effects exhibited by the pitch technology in these two regions to offer beneficial effects to VAWT performance.

(d) pitch curves that are characterized by periodicity, continuity and first-order derivability.

The VAWT-shape pitch motion is considered as a scheme that fits the motivation of the above study. The VAWT-shape pitch not only achieves continuous pitching, but also its pitch law is naturally related to the rotation parameters (TSR and azimuth angle). Several literatures have already studied the VAWT-shape pitch oscillation motion. For example, Tsai et al [46] used VAWT-shape pitch oscillation motion for the first time to study the airfoil dynamic stall. Brunal et al [47] compared the dynamic stall of sinusoidal-shape and VAWT-shape pitch oscillation, and found that sinusoidal-shape pitch overestimates the relationship between lift and AoA in the upstroke. Hand et al [48] applied VAWT-shape pitch on a single blade to compare the dynamic stall characteristics at different TSR. Currently, no study has been conducted on using VAWT-shape pitch oscillation as a VAWT pitch control technique. Therefore, this presents a great opportunity to use the VAWT-shape pitch as a novel pitch strategy.

In this study, the aerodynamic performance of a VAWT was calculated using STAR CCM+ computational fluid dynamics software. The URANS was chosen for the numerical simulation of the unsteady flow field, and the SST k-ω model was used as the turbulence model. By analyzing the variation law of the AoA with the azimuth angle of the zero-pitch blade in one rotation cycle, a pitch control strategy is proposed to proportionally vary the blade AoA under different azimuth angles based on the VAWT type pitch motion. The purpose of this approach is to significantly change the blade AoA when it is large, while in reality it hardly changes when the blade AoA is small. The proposed method enables the AoA at each azimuth to be reduced proportionally so that a VAWT operating at low TSR can have an AoA at higher TSR. This approach greatly improves the power coefficient of the VAWT at low TSR and thus enhances its self-start performance.

The novelty of this study can be summarized as follows:

1. In the existing literature, research on VAWT-type pitch motion has been carried out only in the field of dynamic stall for single airfoil. The application of VAWT-type pitch law to VAWT pitch technology is still not explored. In this work, the effect of VAWT pitch on the performance of VAWT and its effect are analyzed in a more comprehensive way for the first time.

2. The pitch scale factor (μ) is introduced and 10 pitch angles (6 selected for μ>0 and 4 for μ<0) are determined according to TSR at an increment of 0.1. This allows a more detailed understanding of how the aerodynamic performance of the VAWT changes when μ is varied.

3. The existing literature focuses on the construction of pitch angle curves, while this study deepens the understanding of pitch angle curves in terms of the blade pitch angular velocity (first order derivative of the blade pitch equation with respect to time). This provides new ideas for subsequent improvement of the pitch angle curves.

4. The current research on the application of different pitch curves to the windward and leeward regions is mainly concerned with the continuity of the curves themselves. This study describes the characteristics of the pitch curve, which is derived based on that the first-order derivative of the pitch angle curve and it needs to be continuous. It should be noted that intense transient load fluctuations occur when the first-order derivative is not continuous. Fitting the curve following this feature can significantly reduce the fluctuations.

The remaining parts of this paper are organized as follows. Section 2 introduces the aerodynamic parameters of the VAWT. In Section 3, the principle of the novel pitch control strategy proposed is explained. The grid and time step independence of the numerical model is verified in Section 4 and compared with the experimental data. In Section 5, the control effect of the new pitch strategy is analyzed and the combinations of different pitch scale factors are discussed. Finally, the conclusions of this study are presented in Section 6.

2. Aerodynamic parameters of pitch

The relationship between the velocity triangle and the force vector at a certain azimuth angle for the VAWT blade pitch is shown in Fig. 1. The incoming wind speed is U_∞. The blades are arranged in a circle of radius, R. The velocity V is the tangential velocity vector of the rotor. The synthetic velocity W is the relative velocity consisting of the induced velocity (U) and the tangential velocity (V) of the blades. The AoA is the angle between the relative wind speed (W) and the chord of blade. The AoA of the blade without pitch is α, and the AoA after pitch is β. The pitch angle (α_p) of the blade is defined as follows.

$$\alpha_p = \alpha - \beta \tag{1}$$

where α_p is the angle of chord rotation after blade pitching. It is clear that the theoretical AoA (α) and relative wind speed (W) vary with azimuth (θ) and are different at each azimuth.

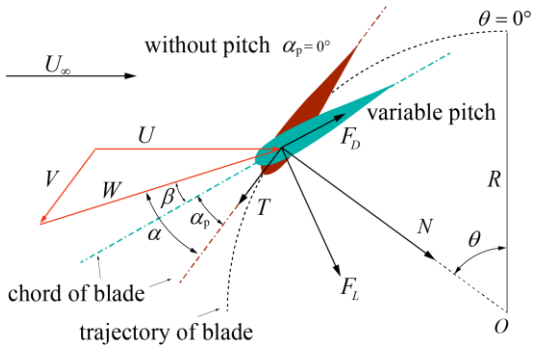

Fig .1. Relationship between force vector and velocity triangle of a VAWT blade

For a VAWT blade, lift (F_L), drag (F_D), normal force (N) and tangential force (T) are the main forces acting (as in Fig 1) on it. The magnitude and direction of lift and drag forces depend on the azimuth of the blade. The blade lift and drag forces are expressed as [49]:

$$F_L = 1/2 C_L \rho W^2 c \tag{2}$$

$$F_D = 1/2 C_D \rho W^2 c \tag{3}$$

where ρ is the density (1.225kg/m^3), and c is the blade chord length. The tangential force (T) can be used to evaluate the performance of the VAWT [49]. The T after pitch can be expressed as:

$$T = R\left(F_L \sin(\alpha - \beta) - F_D \cos(\alpha - \beta)\right) \tag{4}$$

Tip speed ratio (TSR or λ) is an essential dimensionless parameter of VAWTs, and wind speed is a key factor in determining TSR [50] based on Equation (5).

$$\lambda = \omega R / U_\infty \tag{5}$$

where ω is the rotate speed of the VAWT rotor, and R is the radius of wind wheel. The theoretical AoA (α) for a VAWT without pitch defined using Equation (6) [51]:

$$\alpha = \arctan\left(\frac{sin(\theta)}{cos(\theta) + \lambda}\right) \tag{6}$$

Fig. 2 shows the variation of AoA with azimuth angle in a rotational cycle. The AoA of VAWTs blade changes continuously within a period of 360° (2π) and the maximum AoA for λ = 1.25, 1.5, and 1.75 are 53°, 41°, and 34°, respectively. When the AoA increases during rotation, the blade reaches a state of deep stall. This heightened flow separation intensifies, preventing the blade from generating stable lift, ultimately leading to a reduced power coefficient [52,53].

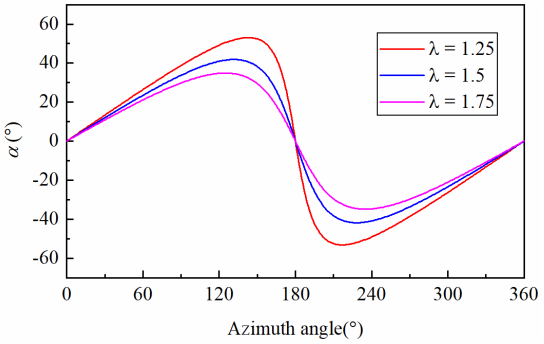

Fig. 2. Variation of AoA with azimuth angle at different TSRs

For VAWTs with low TSRs, a large negative torque is generated due to the large variation of AoA in the rotation cycle. Therefore, this confirms that altering the blade pitch is the most direct way to change the AoA, and the effect increases lift and reduces drag.

3. Novel pitch control strategy

To achieve the desired blade pitching with the variation law of AoA requires finding the first order derivative of time (t) using Eq. 6. Where $\theta = \omega \cdot t$, represents the relationship between rotor rotation speed (ω) and azimuth angle (θ). The variation law of the blade angular velocity is obtained and denoted as $\dot{\alpha}$.

$$\dot{\alpha}(t) = \frac{\omega(1 + \lambda \cos \omega t)}{1 + 2\lambda \cos \omega t + \lambda^2} \tag{7}$$

Assuming that λ is constant, then $\dot{\alpha}$ is a function of the period for 2π. The pitch angle α_p and blade pitch angular velocity $\dot{\alpha}_p$ are denoted as:

$$\begin{aligned} \alpha_p &= \mu \cdot \alpha \\ \dot{\alpha}_p &= \mu \cdot \dot{\alpha} \end{aligned} \tag{8}$$

where μ ($-1 < \mu < 1$) is pitch scale factor, hence, the blade with angular velocity for $-\mu \cdot \dot{\alpha}$ around the aerodynamic center to achieve pitch motion. The use of this pitch law ensures that the pitch angle not only pitches dynamically with the VAWT rotation parameters (λ and θ), but also achieves

a proportional variation.

Fig. 3 shows the pitch direction of the blade in the windward and leeward regions when μ takes positive or negative values. At μ>0, the blade turns clockwise, and at μ<0, the blade turns counterclockwise. In addition, the blade pitch angle is 0 at θ= 0° (360°) and 180°, regardless of the value of μ.

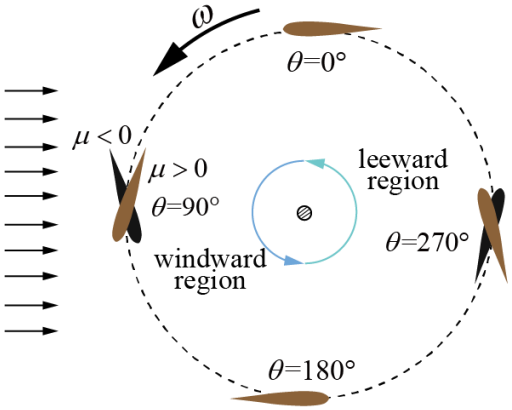

Fig. 3. Pitch diagram of blades at different azimuth angles

To visualize the pitch angle at different azimuth angles. Fig. 4 shows the pitch angle variation curves at different μ for TSR of 1.5. At μ = 0, the blade does not pitch. The pitch angle curve at μ = 1 is the same as the AoA with TSR is 1.5, and the AoA at each azimuth angle after pitching is 0. The pitch angle varies proportionally when μ takes the remaining values. Fig. 5 shows the blade AoA curves at different μ for TSR of 1.5. At each azimuth angle, the blade AoA decreases proportionally with increase in μ. The blade AoA is gradually distributed around the stall AoA. The blade AoA is unchanged at μ = 0, and the blade AoA is 0 at all azimuths at μ = 1. By changing μ, it is found that the maximum AoA gradually decreases with increase in μ. The maximum AoA for different μ is shown in Table 1.

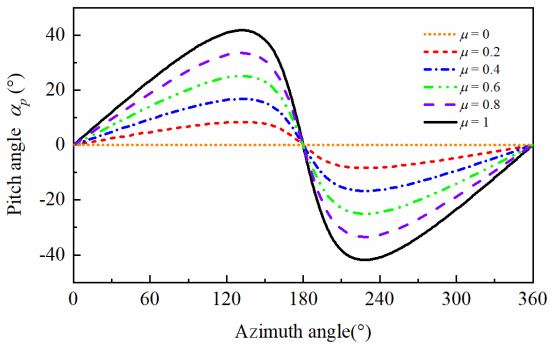

Fig .4. Pitch angle for different μ when TSR is 1.5

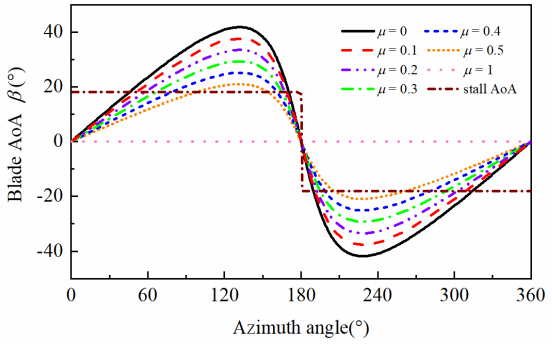

Fig .5. Variation of blade AoA under different μ when TSR is 1.5

Table 1 The maximum AoA with different μ

Pitch scale factors	λ =1	λ =1.5	λ =2
without pitch (μ = 0)	90°	41.81°	30°
μ =0.1	81°	37.63°	27°
μ =0.2	72°	33.45°	24°
μ =0.3	63°	29.27°	21°
μ =0.4	54°	25.09°	18°
μ =0.5	45°	20.91°	15°

The sinusoidal-shape pitch strategy is a more studied continuous pitching technique in VAWT [37,38,54]. The novel pitch strategy and sinusoidal pitch strategy with the same amplitude are compared at a TSR of 1.5, as shown in Fig. 6. The curves are centrosymmetric, so only the differences from 0-180° are investigated. The peak position of the novel pitch strategy (μ=0.3) is significantly deviated closer to the 180° side compared to the sinusoidal pitch motion, which leads to a significant reduction in the blade AoA around the azimuth after pitching. The application of the sinusoidal-type pitch strategy resulted in an excessive reduction in the blade AoA from 0-60°, while the blade AoA could not be effectively reduced around 150°.

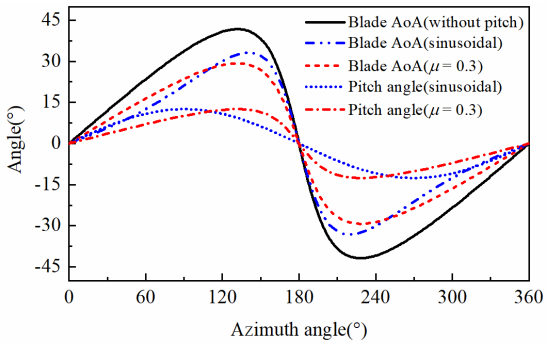

Fig. 6. Comparison of different pitch control strategies and blade AoA when TSR is 1.5

4. Computational Modeling and Verification

4.1 VAWT model and grids

In this study, a straight-blade H-type Darrieus VAWT is considered [55]. The 3-D and 2-D model geometry of the three-bladed VAWT are shown in Fig 7. The blades are arranged in a circle of radius R and rotate at a speed of ω. The main parameters of VAWT are shown in Table 2.

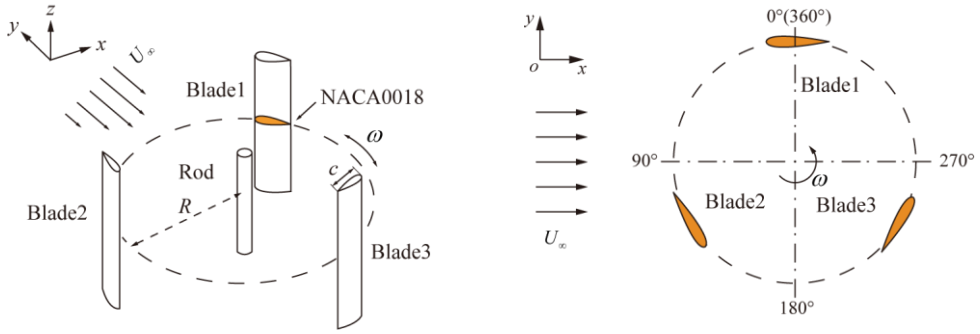

(a) (b)

Fig. 7. VAWT geometric model for (a) 3-D and (b) 2-D

Table 2. Geometric and property parameters of the VAWT

Property / symbol	Value	Unit
Number of blades / N_{VAWT}	3	-
VAWT diameter of wind wheel / D	0.8	m
Height of blade / H	0.8	m
Chord length / c	0.2	m
Diameter of rotor / D_r	0.02	m
Setting angle / γ	0	°
Reynolds number / Re	1.067×10^4	-
Incoming wind speed / U_∞	8	$m\cdot s^{-1}$
Blade solidity / σ	0.75	-

Balduzzi et al [56] found that 2-D CFD simulations, although based on simplified computational domain, are still sufficient to accurately describe the flow field around the wind turbine. Therefore, considering the large number of cases in the work, the 2-D model with NACA0018 airfoil is used as the study object to reduce the computational cost.

The computational domain sizes and boundary conditions of the VAWT are shown in Fig 8. The computational domain is a rectangle of 45D × 30D (referenced to the work of Elkhoury [55]) and has three subdomains: the blade domain, the rotational domain, and the far-field domain. The interface between the rotation domain and the far-field domain is non-conformal, by sliding grids to allow rotation. The motion of the rotation domain enables numerical simulations to be conducted at different TSRs. The incoming flow direction is set at the velocity inlet and the wake dissipation direction is set at the pressure outlet.

Fig. 9 shows the details of the VAWT grid distribution. The grids are polyhedral cells generated by STAR-CCM+. In order to accurately calculate the effect of viscous bottom layer on the blade surface, the first grid height of the airfoil wall boundary layer is set at 0.01 mm to ensure that the y^+ value is less than 1. The total thickness of the boundary layer is 2.5 mm with the growth ratio of 1.12. In addition, the 2D × 4D rectangular region grids around the rotation domain are refined.

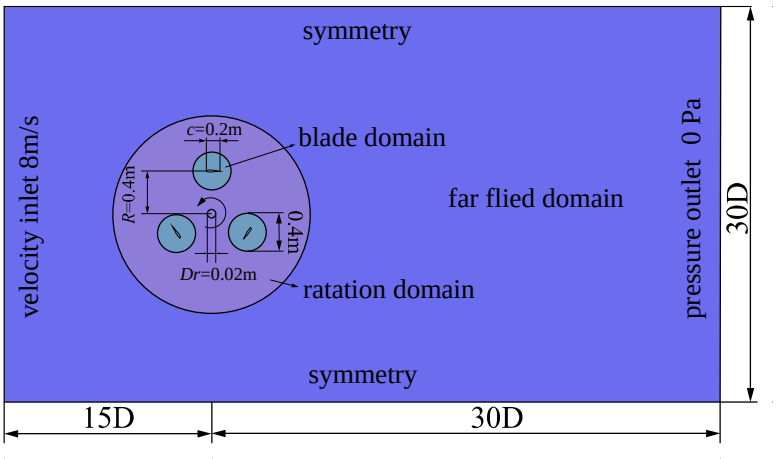

Fig. 8. Calculational domain size and boundary conditions

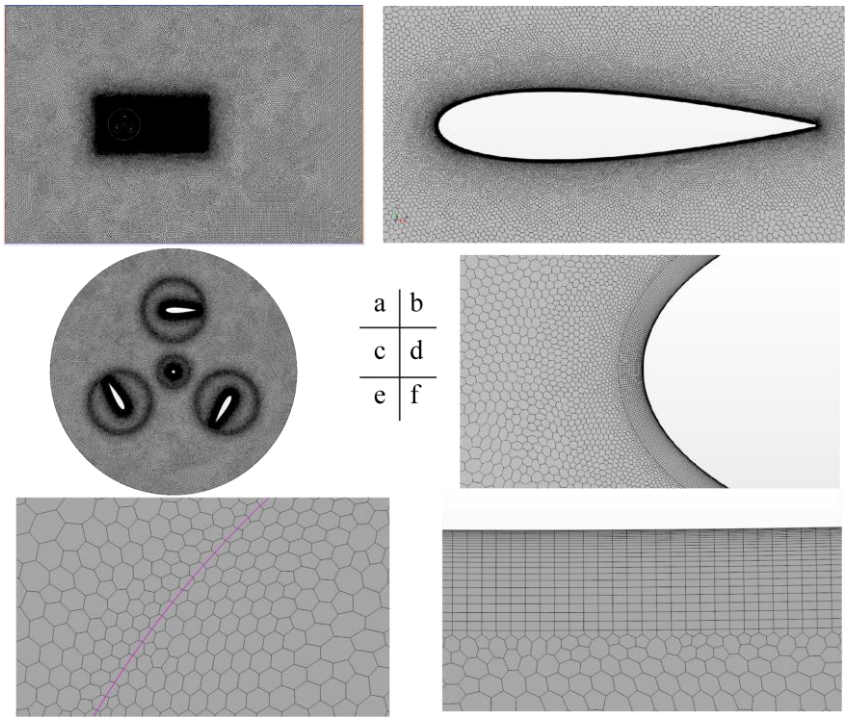

Fig. 9. Grid distribution around the VAWT: (a) the full computational domain, (b) the blade, (c) the rotation domain, (d) the leading edge, (e) the interface and (f) the boundary layer

4.2 Computational Models

In this study, the inlet velocity is set at less than the local sound velocity and the fluid is considered incompressible. The unsteady Reynolds averaged navier-stockes (URANS) equation is solved using STAR-CCM+ simulation software. Considering the small Mach number and no thermal diffusion, the incompressible implicit separated flow model is used. The pressure-velocity equation is coupled using SIMPLEC algorithm. The convective flux is calculated using the second-order windward format.

For flow field models, the SST *k-ω* turbulence model has a better computational accuracy for free shear turbulence, boundary layer attached flow and moderate separated flow [57]. This is usually regarded as suitable for simulating the H-type VAWT [58]. Belamadi et al [59] compared different turbulence models (Standard *k-ε*, Standard *k-ω*, SST *k-ω* and Spalart-Allmaras) with experimental data and showed that the SST k-*ω* model agrees better with experimental results. Ma et al [60] and Orlandi et al [61] also obtained satisfactory power and torque results within the allowed error. Therefore, the SST *k-ω* model is chosen for the numerical simulations in this section. The governing equations are as follows:

$$\frac{\partial(\rho k)}{\partial t}+\frac{\partial(\rho u_i k)}{\partial t}=P_k-\tau_{ij}\frac{\rho k^{3/2}}{l_{k-w}}+\frac{\partial}{\partial x_i}\left[\left(\mu+\frac{\mu_t}{\sigma_k}\right)\frac{\partial k}{\partial x_i}\right] \tag{9}$$

$$\frac{\partial(\rho\omega)}{\partial t}+\frac{\partial(\rho u_i\omega)}{\partial x_i}=\alpha_2\frac{\omega}{k}P_\omega-\beta_2\rho\omega^2+\frac{\partial}{\partial x_j}\left[\left(\mu+\frac{\mu_t}{\sigma_{\omega^2}}\right)\frac{\partial k}{\partial x_i}\right]+2\rho(1-F_1)\sigma_{\omega^2}\frac{1}{\omega}\frac{\partial k}{\partial x_i}\frac{\partial \omega}{\partial x_i} \tag{10}$$

where P_k and P_ω are turbulence generators. F_1 is the mixing function. σ_k, α_2, β_2 and $\sigma_{\omega 2}$ are constants with values of $\sigma_k = 2$, $\alpha_2 = 0.44$, $\beta_2 = 0.0828$, and $\sigma_{\omega 2} = 0.856$, respectively. τ_{ij} is the viscous force, μ is the laminar viscosity coefficient, μ_t is the eddy viscosity coefficient, k is the turbulent kinetic

energy, and ω is the dissipation rate. Details of this equation are given in reference [43].

4.3 Grids and the time step independence studies

The power coefficient of VAWTs is an important index reflecting the aerodynamic performance. It can be defined by the torque coefficient and TSR as follows [62].

$$C_T = T \Big/ \left(0.5\rho U_\infty^2 AR\right) \tag{11}$$

$$C_P = C_T \cdot \lambda \tag{12}$$

where T is the combined torque of the three blades; C_T is the torque coefficient; C_P a is the power coefficient; and A is the swept area of the wind wheel.

The variation of grid density and time scale affects the accuracy of the CFD calculated results, which increases the dynamic pitching error. Therefore, the grid and time independence need to be studied to determine the appropriate number of grids and time steps to accurately obtain the VAWT's rotational torque.

In order to investigate the influence of grid density on the results, four different grids (G1-G4) are used to calculate the C_P. Table 3 shows the details of the parameters of the four grids. The aim is to select the most suitable grid to ensure the least amount of computational effort.

Table 3. Details of the four grid parameters

Grid	Number of elements	Boundary Layer		Global growth rate	Interface element size	
	N_E	y/c (10^{-5})	N_N	G_R	$\Delta I_B/c$	$\Delta I/c$
G1	330166	9.324	2315	1.08	0.0188	0.0563
G2	393544	7.136	2968	1.06	0.0163	0.0487
G3	432657	5.762	3254	1.04	0.0150	0.0450
G4	481999	4.598	3747	1.02	0.0137	0.0413

The C_P was calculated using the URANS solver for 15 rotation cycles and the last cycle was selected for validation. To minimize the sensitivity of the run parameters to the C_P, A grid independence verification was conducted for three TSRs. Fig. 10 shows the variation of C_P for different TSRs. The aerodynamic coefficients converge gradually as the number of grids increases.

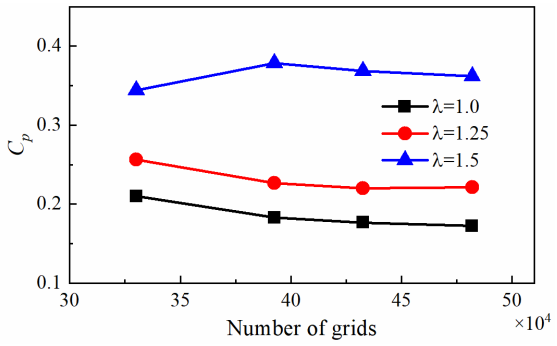

Fig. 10. Results of grid independence verification at different number of grids

For grids with different densities, the difference in C_p is calculated and defined as $\Delta\varepsilon_{g+1,g}$:

$$\Delta\varepsilon_{g+1,g} = \left|\left(C_P\right)_{g+1} - \left(C_P\right)_g\right| \quad (g = 1,2,3) \tag{11}$$

Where, g denotes the number of Grid. As the number of grids increases, the relative rate of change $\Delta e_{g+1,g}$ of C_p is expressed as follows:

$$\Delta e_{g+1,g} = \left| \frac{\Delta \varepsilon_{g+1,g}}{(C_P)_g} \right| \times 100\% \quad (12)$$

Table 4 shows the results of the relative rate of change of grid sensitivity for four grid numbers at three TSR (λ = 1.0, 1.25, 1.5). Under different TSR, the relative rate of change of C_p decreases with increase in the number of grids. Compared with G1, when the grid number increases to G2, the relative change of C_p exceeds 5%. The relative rate of change of C_p for G3 is less than 3% compared with G4, indicating that continuously increasing the grid number has less influence on the calculated results. Therefore, the grid number of G3 is chosen.

Table 4. Results of relative rate of change of C_P at different TSR

λ	$\Delta\varepsilon_{2,1}$	$\Delta\varepsilon_{3,2}$	$\Delta\varepsilon_{4,3}$	$\Delta e_{2,1}$	$\Delta e_{3,2}$	$\Delta e_{4,3}$
1.0	0.0268	0.0064	0.0041	10.8%	3.65%	2.32%
1.25	0.0299	0.0068	0.0015	5.09%	3.11%	1.32%
1.5	0.0388	0.0099	0.0067	9.02%	2.42%	1.68%

Three time steps are chosen to study the effect of time sensitivity on the calculation results. Table 5 shows the successively decrease in time steps. Where 0.25°, 0.5° and 1° indicate the rotation angles corresponding to different time steps, respectively. The computation time of each time step in one rotational cycle is an important consideration. The simulation time per cycle is recorded on a 16-core processor using a high-performance computing cluster.

Table 5. Parameters of the time step independence study

Parameters	Time step/ Δt	Rotation angle/ $\Delta\theta$	Simulation time/(hrs/cycle)
T1	$2\pi/360\omega$	1.0°	1.26
T2	$2\pi/720\omega$	0.5°	2.25
T3	$2\pi/1440\omega$	0.25°	4.46

Fig. 11 shows the comparison between the single-blade torque coefficients for one rotational cycle at different time steps. At λ = 1.0, 1.25, 1.5, the time step of T1 causes the C_T to be significantly overestimated in the windward region. In Fig. 11d, the C_P varies by 8.52%, 7.63% and 10.23% for T2 compared to T1. The rate of change of C_P is smaller for T3 compared to T2, 2.11%, 1.58% and 1.67%, respectively. T2 and T3 can provide a better estimate of the force coefficients of the VAWT trend and behavior. However, T3 requires twice as much time as T2 to calculate one rotational cycle. Considering the computational accuracy and the solution period, the time step of T2 is chosen as the most suitable for this study.

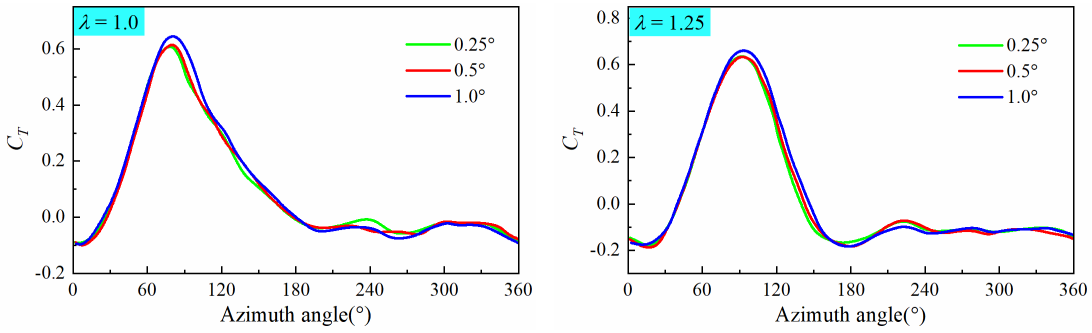

(a) (b)

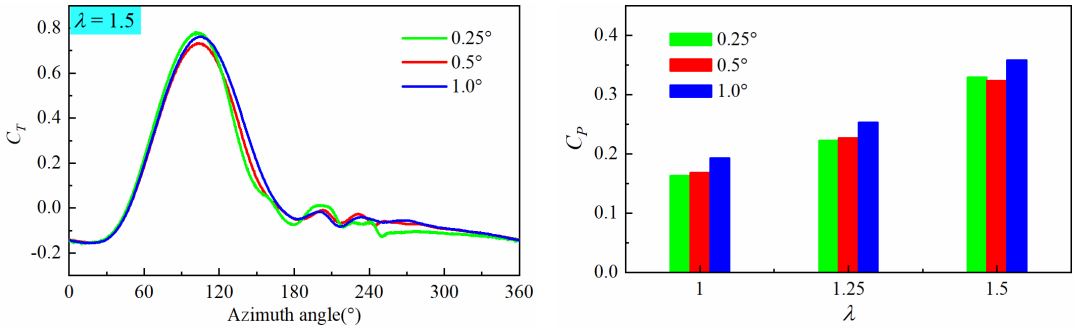

(c) (d)

Fig. 11. Results of time sensitivity verification on the variation of (a) λ = 1.0, (b) λ = 1.25, (c) λ = 1.5 and (d) average C_p at different time steps

4.4 Comparison of CFD results and experimental data

To verify the reliability of the calculated results in this paper, the variation of the VAWT blade power coefficient (C_P) was compared with experimental data [55], 3-D CFD numerical results [60] and 2-D CFD results [53], as shown in Fig. 12. Comparing the experimental data with 2-D and 3-D CFD results, the 2-D CFD results show good agreement at low TSRs, but large differences at high TSRs were observed. The difference in numerical results is mainly due to the fact that the 2-D numerical model neglects the blade tip loss, the 3-D rotational effect and the influence of the support members on the aerodynamic performance of the blade. According to the Refs [63], the overprediction of performance by up to 32% for the 2-D simulation is acceptable compared to the 3-D CFD simulation. Although the numerical results in this study predict a much higher C_p at high TSR, the main flow trends have been captured. Therefore, the simulation results are reliable.

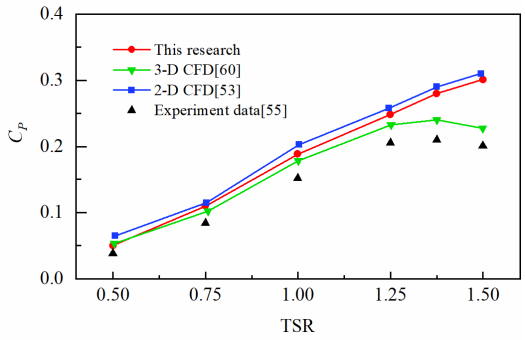

Fig. 12. Comparison of calculated values of *Cp* with experimental data

5. Results and Analysis

5.1 Aerodynamic analysis

A fixed wind speed of 8 m/s is used to simulate different TSRs by varying the blade rotation speed. Fig. 13 shows the C_P of VAWT at different TSRs for continuously increasing μ. In the simulated TSR range, the C_P increases the most at μ = 0.3. The range of AoA is inversely proportional to the TSR. At a TSR of 1.25, the AoA operates in the range between +53° and -53°. However, at TSR of 1.5, this range decreases by about 10°, with the operating range of AoA being between +41° and - 41°. When the TSR is set at 1.25, a value of μ = 0.1 results in the blade being AoA equal to the AoA observed at a TSR of 1.5. As μ increases, the blade AoA continuously

decreases, and the C_P exhibits an increase followed by a decrease at different TSRs. The increment in C_P at low TSR is significantly better than that at a high TSR when μ is the same. Table 6 shows the growth rate of C_P at different TSRs compared with the original VAWT. The C_P of the VAWT is significantly increased by using the novel pitch strategy, especially when the growth rate reached 146% at TSR of 1.25, which enhanced the wind catching ability of the blades and improved the self-starting capability of the VAWT.

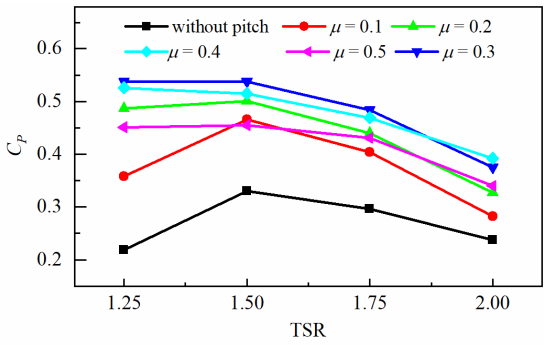

Fig. 13. Results of C_P at different TSRs for continuously increasing μ

Table 6 Comparison of C_P between novel pitch strategy and without pitch

TSR	C_P (μ =0)	C_P (μ =0.3)	Growth rate
1.25	21.8%	53.7%	146%
1.5	34.9%	53.8%	54.2%
1.75	31.6%	48.3%	52.8%
2	25.7%	37.5%	45.9%

The maximum C_P was obtained at a TSR of 1.5. To further illustrate the effect of the novel pitch strategy at different azimuths, a comparison of the C_P of the VAWT at μ = 0.3 and without pitch is shown in Fig. 14. The C_P at μ = 0.3 is improved in all azimuths, especially around the three azimuths of 38°, 167.5° and 278.5°. Moreover, the C_P for μ = 0.3 is greater than 0 in all azimuths, which indicates that this pitch strategy improves the aerodynamic performance of the VAWT in all azimuths during one rotational cycle.

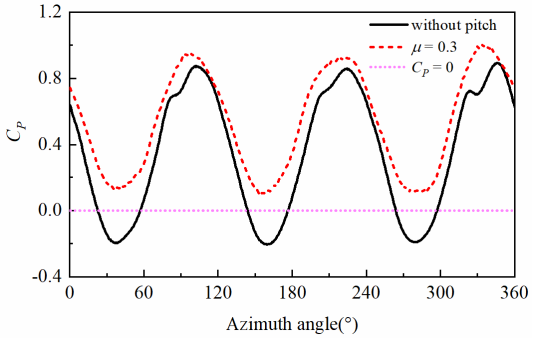

Fig. 14. Comparison of C_P between μ =0.3 and without pitch at TSR of 1.5

Although the C_P increased during one rotational cycle, the least increment was observed around the azimuths of 113.5°, 226.5° and 350° in Fig. 14. The difference in azimuthal position among 38°, 167.5° and 278.5° is about 120° (the same for 113.5°, 226.5° and 350°), which is due to the similarity in motion pattern of the three blades in one rotational cycle. Therefore, it is only necessary to analyze the flow field at 38° and 113.5° azimuths, and thus to understand why the C_P increases significantly at 38°, 167.5° and 278.5° azimuths, but with almost no effect at 113.5°, 226.5° and

350° azimuths.

Fig. 15 shows the vorticity contours of the VAWT flow field at different azimuth angles for μ=0 and μ=0.3 at TSR of 1.5. It is observed that the pitch causes the wake vortex shedding of the VAWT to be broken from large vortex to small and fine vortices, which avoid the continuous development of shedding vortices to become larger and consume more energy. Compared with the local enlarged view of blade 2 in Fig. 15(a), for the VAWT without pitch control, the blade 2 has a strong flow separation after a rotation through 38°. Blade 1 is affected by vortex shedding at the trailing edge of blade 2. After applying the pitch control, the flow separation at the leading edge is suppressed because the AOA of blade 2 is reduced. Consequently, blade 1 is less affected by the wake of blade 2. The pitch improves the flow state of blades 1 and 2. From Fig. 15(b), it can be observed that in a VAWT configuration without pitch control, both blade 2 and blade 3 experience the effects of trailing edge shedding vortex when the rotation reaches 113.5°. Notably, the trailing vortex encountered by blade 2 is more pronounced compared to blade 3. After applying pitch control, blade 3 is still affected by the trailing edge vortex shedding of the front blade. However, blade 2 is no longer affected by the vortex, and the vortex shedding is small. The pitch at this rotational angle has a limited suppression effect on flow separation.

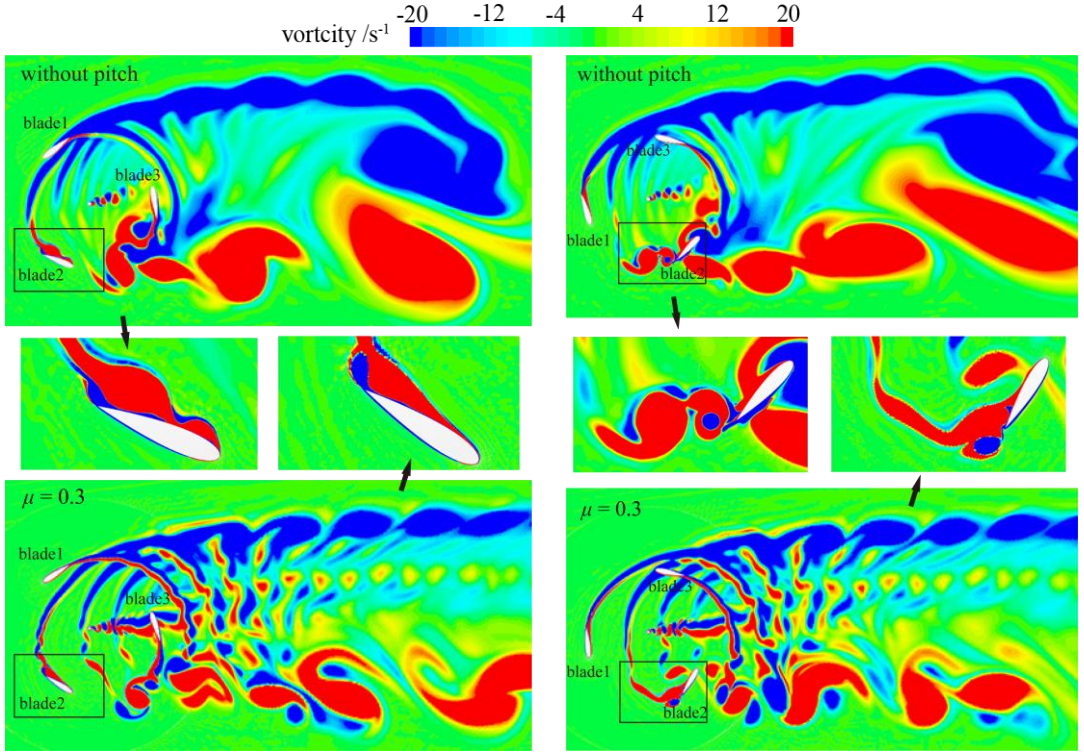

(a) (b)

Fig. 15. Comparison of the vorticity contours of (a) 38° and (b) 113.5°azimuth angles for VAWT

The vorticity contours offer a visual representation of the intricate details within the flow field, allowing for a microscopic analysis. Conversely, the pressure distribution along the surface of the VAWT blades during pitching provides a quantitative assessment for the blade's aerodynamic performance. Therefore, Fig. 16 shows the pressure coefficient of the three blades along the chord length direction when the VAWT is rotated by 38° and 113.5°.

From Fig. 16(a), the variation of pressure coefficient in blade 1 is not obvious when the VAWT is rotated through 38°. The pressure difference between the two surfaces of the blade without pitch is slightly larger because of the trailing edge vortex shedding from the front blade. A severe flow

separation in blade 2 is observed, which causes the pressure coefficient at the suction surface to exceed the pressure surface at 30%-50% of the chord length. As a result, there is not enough pressure difference in blade 2 to provide rotational torque. The pitch suppresses the flow separation at the suction surface, which increases the leading edge pressure difference and reverses the negative pressure difference. The pressure coefficient curve of blade 3 has an "∞" shaped cross. This is due to the alternation between the pressure surface and the suction surface of the VAWT in the leeward region, where the trailing edge of the blade produces a negative torque. The pitch produces more negative torque because blade 3 is influenced by the trailing flow of the front blade. However, the magnitude of the negative torque is much less than the positive torque provided by blade 2. In total, at this rotational angle, it is the pitch that reverses the pressure difference of blade 2, and therefore significantly increases the output torque of the VAWT.

When VAWT is rotated through 113.5°, the AoA of blade 1 is greater than the stall AoA both at $\mu = 0.3$ and without pitch. Therefore, observing from Fig. 16(b), there is almost no difference in pressure coefficient of blade 1. Without pitch, blade 2 is affected by the trailing edge vortex shedding of blade 3, which causes a significant fluctuation of the pressure coefficient curve at the trailing edge. By adjusting the pitch, blade 2 becomes unaffected by the vortex shedding created by the front blade. As a result, the pressure coefficient tends to exhibit a smoother behavior. However, the pressure difference between the two surfaces of the blades does not increase while the AoA of blade 3 is smaller than the stall AoA. The AOA becomes smaller after pitching, which resulted in a smaller lift force. As a result, the pressure difference between the two surfaces of the blades becomes smaller. However, this azimuth produces a negative torque. The pitch reduces the negative torque, which is beneficial to the VAWT. In summary, the pitch stabilizes the pressure fluctuations on both surfaces of the blade at this rotational angle. However, the pressure difference between the two surfaces of the blade hardly changes, so the output torque of the VAWT does not change significantly.

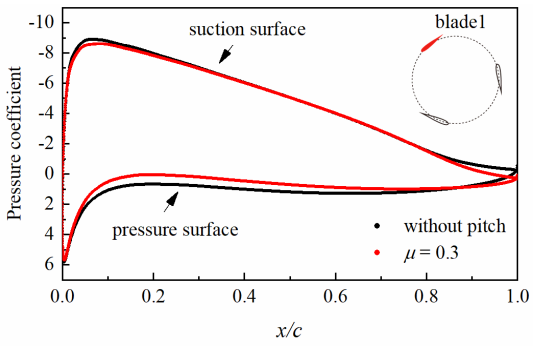

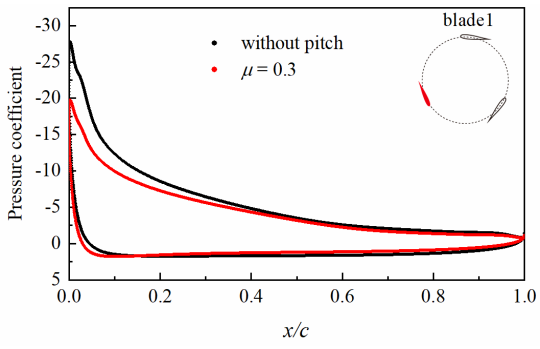

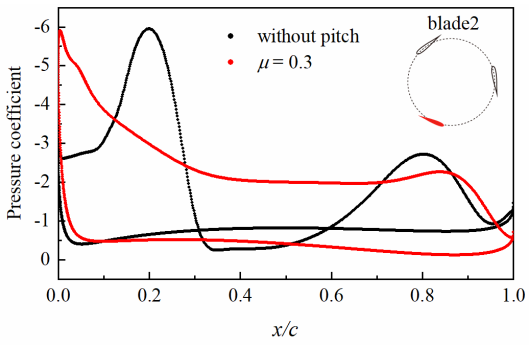

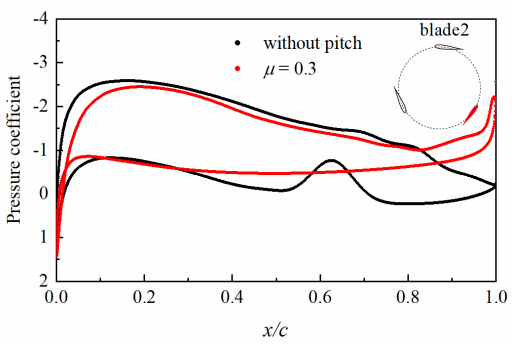

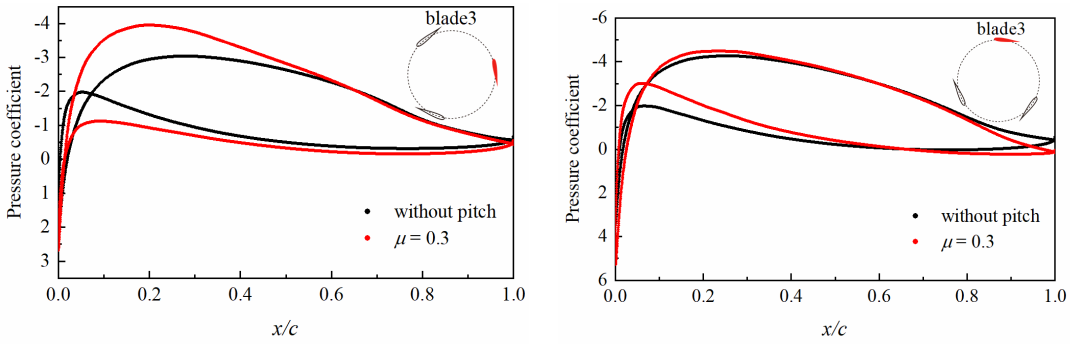

Fig. 16. Comparison of pressure coefficients of three blades at (a) 38° and (b) 113.5° azimuth angles

Fig. 17 shows the comparison of C_P for sinusoidal pitch and novel pitch strategies with the same magnitude when TSR is 1.5. As μ increases, the C_P increases and then decreases. At μ = 0.3, the C_P of the sinusoidal pitch strategy starts to decline compared to the VAWT without pitch. At μ = 0.5, the application of the sinusoidal pitch strategy causes the VAWT aerodynamic performance to deteriorate, resulting in the C_P becoming less than 0. Compared with the sinusoidal pitch strategy, the novel pitch strategy used in this study has a larger AoA control range and better control effect, which offers a more excellent pitch strategy.

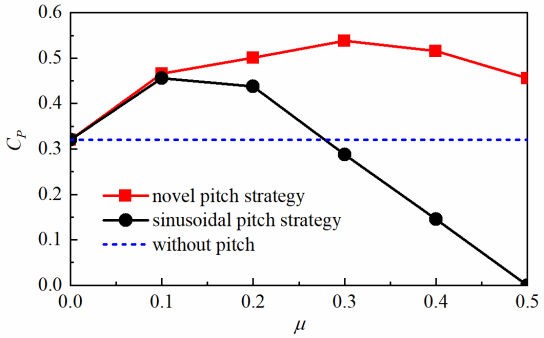

Fig. 17 Comparison of C_P between the novel pitch strategy and the sinusoidal pitch strategy when TSR is 1.5

5.2 Parameter combinations of μ

The use of the same μ at 0-360° significantly enhances the C_P of the VAWT. The simulation results in Ref [32] show that the effect of the pitch on the C_T of the VAWT is different in the windward (0-180°) and leeward (180-360°) region. Therefore, it is necessary to understand the control law of the parameter μ for the windward and leeward regions to obtain their respective optimal pitch angle. Fig. 18 shows the single blade C_T at $\mu > 0$ and $\mu < 0$ for a TSR of 1.5.

From Fig. 18, the C_T increases from 0-180° azimuth for $\mu > 0$ and in 180-360° azimuth for $\mu <$ 0. Based on this phenomenon, different μ are applied in the 0-180° and 180-360° azimuth ranges to investigate their coupling enhancement effects on VAWT. Table 7 shows nine dual pitch scale factors (*dpsf*) combination control strategies set up to obtain the effect law of different *dpsf* on the single blade C_T of VAWT.

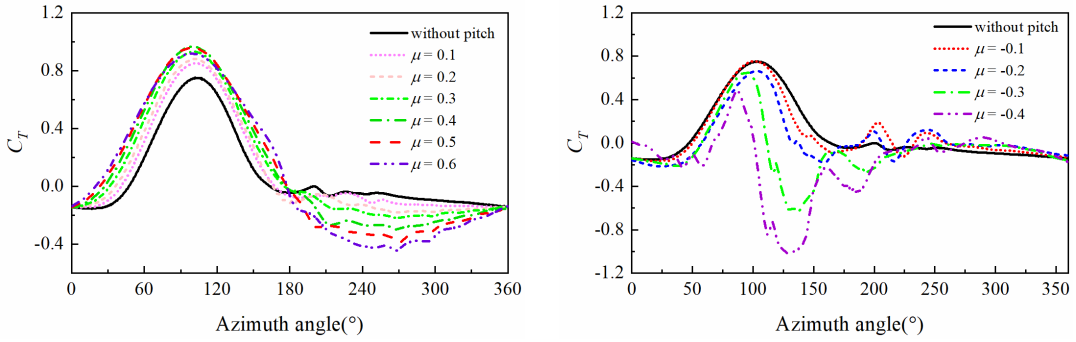

(a) (b)

Fig. 18. Comparison of C_T of (a) μ >0 and (b) μ <0 when TSR is 1.5.

Table 7. Parameters of nine different *dpsf*

dpsf	0-180°	180-360°
[0.3,0.1]	μ =0.3	μ = 0.1
[0.3,0]	μ =0.3	μ = 0
[0.3, -0.1]	μ =0.3	μ = -0.1
[0.4,0.1]	μ =0.4	μ = 0.1
[0.4,0]	μ =0.4	μ = 0
[0.4, -0.1]	μ =0.4	μ = -0.1
[0.5,0.1]	μ =0.5	μ = 0.1
[0.5,0]	μ =0.5	μ = 0
[0.5, -0.1]	μ =0.5	μ = -0.1

The C_T of a single blade is calculated for nine different combinations of *dpsf* and compared with μ = 0.3, and the results are shown in Fig. 19. The *dpsf* pitch strategies, while causing a significant increase in C_T between 180-360°, caused a decrease in C_T within 0-180°. This indicates that increasing C_T within 180-360° suppresses the C_T of 0-180°, and the larger the increase C_T within 180-360°, the stronger the suppression effect on 0-180°. When the same μ is chosen in the 180-360° range, the peak C_T of 0-180° is compared for each combination of control strategies in Figs. 19(a), 19(b), and 19(c). The results show that the reduction is the largest when μ = 0.5, followed by μ = 0.4, while the reduction is smaller when μ = 0.3. In addition, the *dpsf* pitch strategy generates intense transient torque fluctuations at 0° (360°) and 180°.

Fig. 20 shows the comparison of C_T for VAWT at different *dpsf*. Due to the superposition of three blade motions in one rotational cycle, fluctuations are generated at angles of 0° (360°), 60°, 120°, 180°, and 240°. The same μ is used for 0-180°, and the fluctuations are greatest when using μ = -0.1, next for μ = 0, and smallest for μ = 0.1 in the 180-360°. The same μ is used in 180- 360°, and fluctuations are greatest with μ=0.5, next with μ=0.4, and smallest with μ=0.3 in 0-180° azimuth. Selecting different μ in the range of 0-180° and 180-360°, the larger the difference between the two μ, the larger the fluctuation. Observing the local enlarged plots, the C_T around 30°, 150° and 270° azimuths increases with increasing μ.

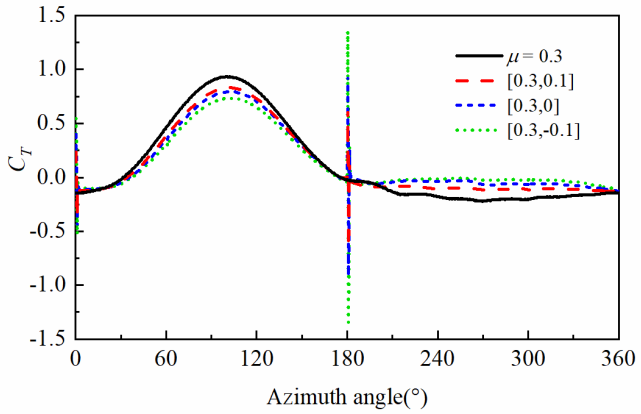

(a)

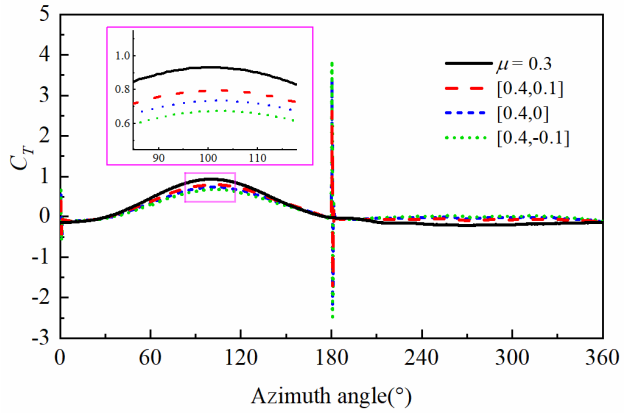

(b)

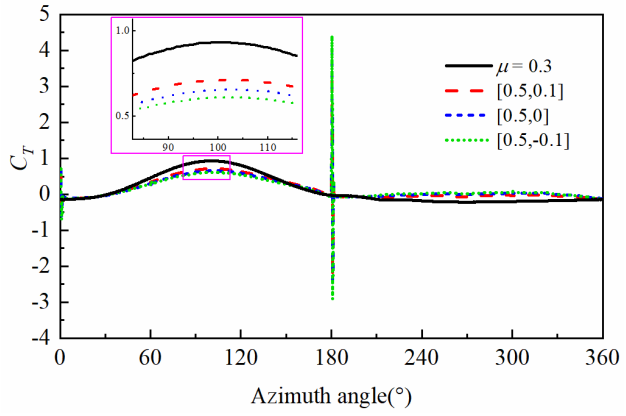

(c)

Fig. 19. Comparison of C_T for single blade with different pitch strategies: (a) μ=0.3, [0.3, -0.1], [0.3,0] and [0.3,0.1], (b) μ=0.3, [0.4, -0.1], [0.4,0] and [0.4,0.1] and (c) μ=0.3, [0.5, -0.1], [0.5,0] and [0.5,0.1]

478

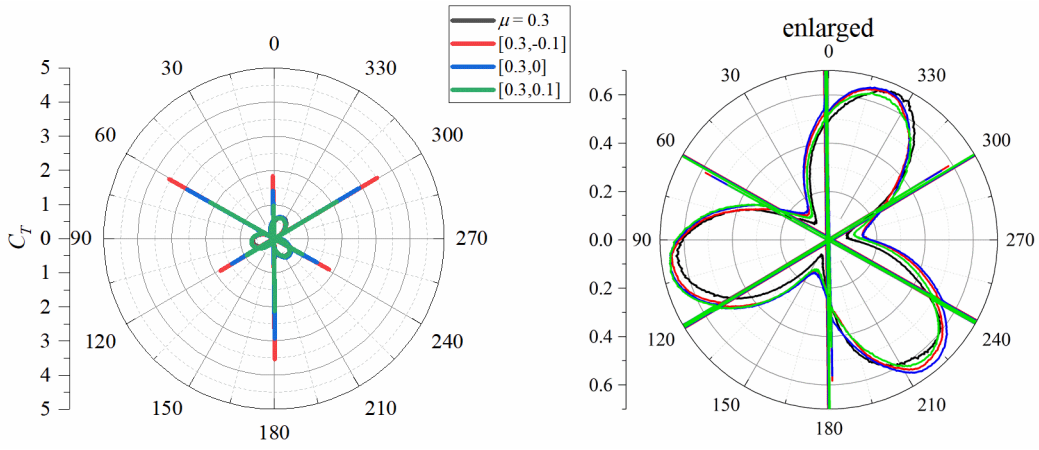

(a)

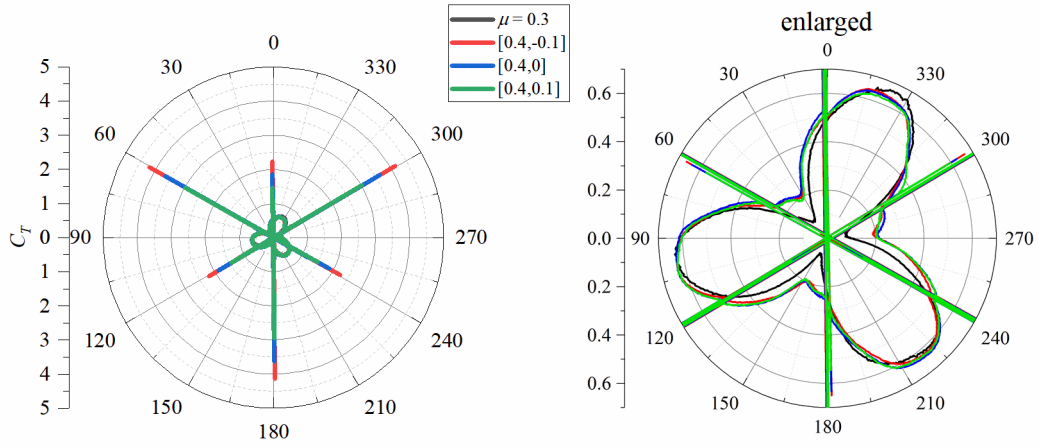

(b)

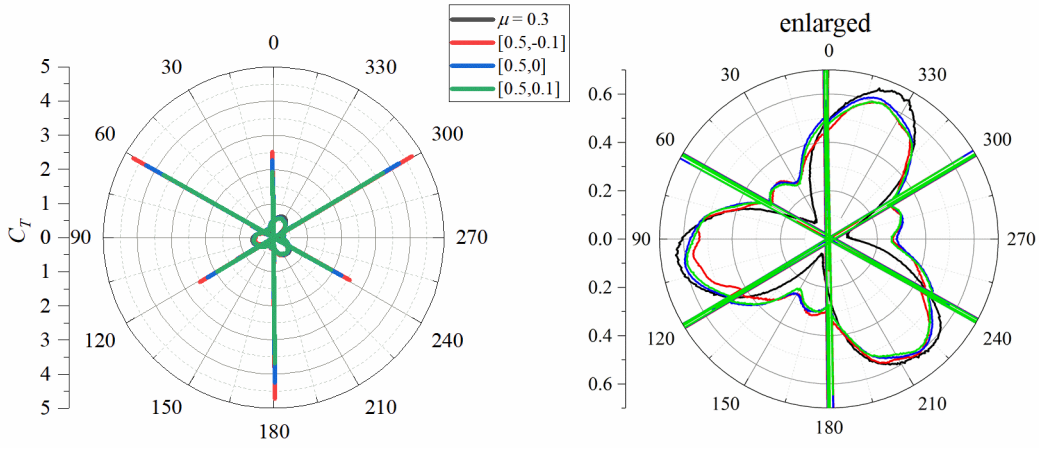

(c)

Fig. 20. Comparison of C_T for VAWT with different pitch strategies: (a) μ=0.3, [0.3, -0.1], [0.3,0] and [0.3,0.1], (b) μ=0.3, [0.4, -0.1], [0.4,0] and [0.4,0.1] and (c) μ=0.3, [0.5, -0.1], [0.5,0] and [0.5,0.1]

The C_T decreased for 0-180° and increased for 180-360° when using the *dpsf* pitch strategy. A change in VAWT performance was not directly observed from the plot of C_T variation with azimuth angle. Therefore, the fluctuation data of 0° and 180° are removed temporarily for further analysis. The average C_T at different *dpsf* for 0-180°, 180-360° and 0-360° is calculated and shown in Fig. 21, while the average C_T is the average C_T of *dpsf* minus the average C_T of μ = 0.3. Although the average C_T decreases in the 0-180° azimuth, the increment of the average C_T in the 180-360° is

greater than the decrease in the 0-180°. This indicates that the nine *dpsf* strategies improved the C_T compared to μ=0.3, with [0.3,0], [0.4,0], [0.4,0.1], and [0.5,0.1] being more effective.

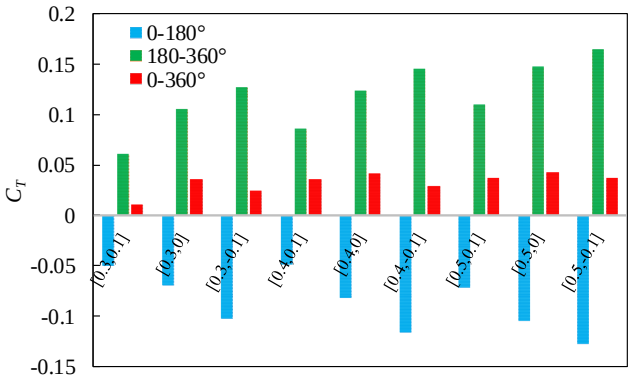

Fig. 21. The average C_T of different *dpsf* at range of 0-180°, 180-360° and 0-360°

The use of *dpsf* causes transient torque fluctuations at 0° and 180° azimuth. This is related to the smoothness of the pitch curve. A similar phenomenon has appeared in the Ref [32], and the study elaborates the reason for its adoption in terms of the pitch angular velocity (first order derivative of the pitch function, denoted as $\dot{\alpha}_p$). Fig. 22 shows the pitch angle curves and angular velocity curves for μ = 0.4, [0.4, -0.1], [0.4,0] and [0.4,0.1]. From Fig. 22(a), although all pitch curves are continuous, the [0.4, -0.1], [0.4,0] and [0.4,0.1] plots with torque fluctuations are not smooth. The pitch curves using *dpsf* have a sharp point at 180° azimuth. From Fig. 22(b), due to the difference in left and right derivatives of the pitch curve at 180° azimuth, the sharp point causes a break in the angular velocity curve. The larger the break distance, the larger the torque fluctuation.

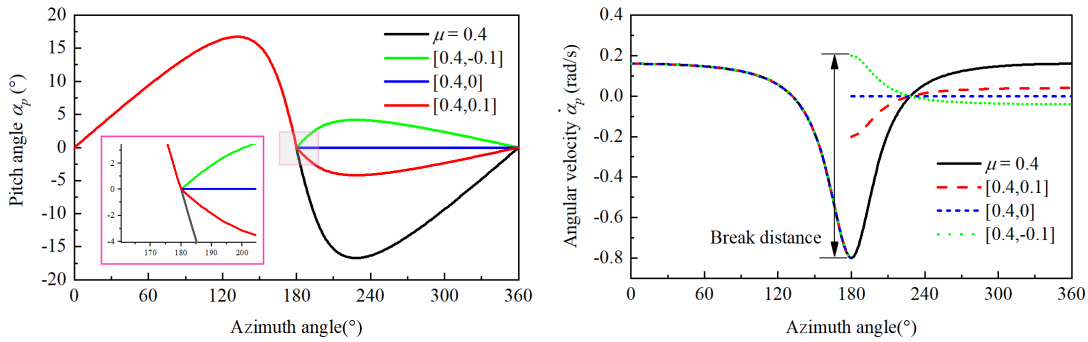

(a) (b)

Fig. 22. Comparison of the curves for (a) pitch angle and (b) angular velocity at μ=0.4, [0.4, -0.1], [0.4, 0] and [0.4, 0.1]

5.3 Pitch angular velocity curve fitting

The blade transient torque fluctuations caused by the change of μ at 0° (360°) and 180° azimuth in the *dpsf* pitch strategy affect the operational stability of the VAWT blade. Therefore, to reduce the torque fluctuation, the pitch function is fitted to the *dpsf* pitch strategy. The fitted pitch function is derived as follows.

$$g(\theta) = \rho_i(\theta) \cdot \alpha_p \tag{13}$$

Where $g(\theta)$ is the fitted pitch function, $\rho_i(\theta)$ is the weight function of the blade at different azimuth angles, and α_p is the original pitch function. The fitted objectives of $g(\theta)$ to be satisfied are as follows:

i) The objective function does not affect the periodicity of the original pitch function and can change the curve only in local azimuth angle.

ii) The curve is continuous and first-order derivable in the azimuth range of 0-360°.

iii) The left derivative is equal to the right derivative at 0° (360°) and 180° azimuths.

The specific implementation is as follows: the pitch curve of 0-180° is unchanged, and the curve of 180-360° is divided into 4 segments. The construction parameters of the weight function are shown in Table 8. Where m, n, l are the coefficients to be determined when μ is determined. The pitch curves of [0.3,0.1], [0.4,0.1], and [0.5,0.1] are chosen for fitting. This is because the average C_T increases in these *dpsf* strategies. Table 9 shows the parameters of the fitted weight functions for the three pitch curves, namely [0.3,0.1]-fitted, [0.4, 0.1]-fitted, and [0.5, 0.1]-fitted.

Table 8. Construction of weight functions at different azimuth angles

Azimuth angle/°	$\rho_i(\theta)$
0-180	1
180-190	$\left((\theta-190)^2/m\right)+2$
190-210	$\left((\theta-210)^2/n\right)+1$
210-300	1
300-360	$\left((\theta-300)^2/l\right)+1$

Table 9. Parameters of weight function for different control strategies

Improvement strategies	0-180	180-360	m	n	l
[0.3, 0.1]-fitted	μ =0.3	μ =0.1	100	400	1800
[0.4, 0.1]- fitted	μ =0.4	μ =0.1	50	400	1200
[0.5, 0.1]- fitted	μ =0.5	μ =0.1	100/3	400	900

The fitted pitch curves are plotted according to the coefficients of each weight function. The [0.4,0.1]-fitted is taken as an example and compared with [0.4,0.1], as shown in Fig 23. The fitted curve becomes smooth at 180° and 360° (in Fig. 23(a)). Compared to [0.4,0.1], the [0.4,0.1]-fitted changes the curve profile only in local azimuths. The breaking distance of the pitch angular velocity curve disappears (in Fig. 23(b)) and then becomes continuous at 180° and 360°.

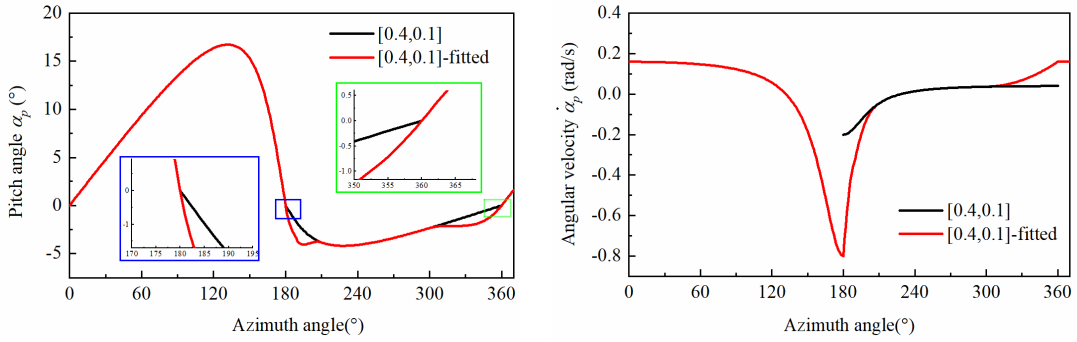

(a) (b)

Fig. 23. Results of the pitch curve fitting in (a) pitch angle and (b) angular velocity at different azimuths

Fig 24 shows the VAWT single blade C_T for three fitted pitch curves and compare to μ = 0.3. The use of the fitted pitch curves resulted in significant reductions in torque fluctuations, with only slight oscillations at 180°. The peak C_T curves for [0.3,0.1]-fitted, [0.4,0.1]-fitted and [0.5,0.1]-fitted all have higher performance than μ = 0.3.

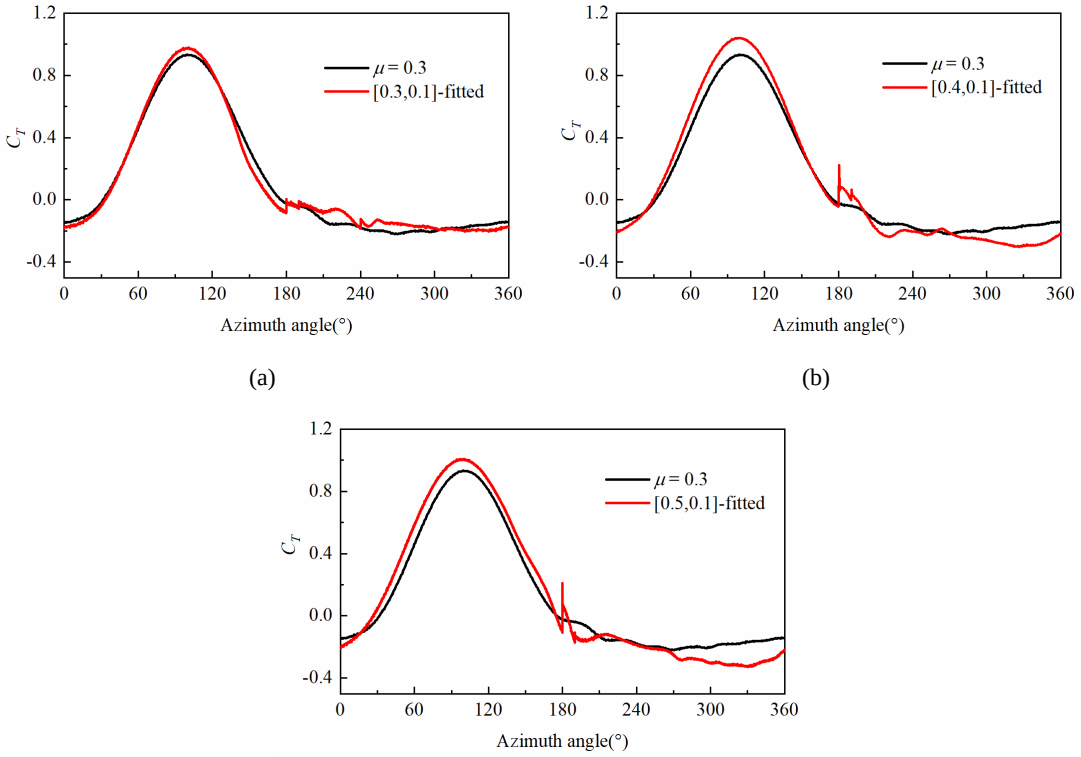

Fig. 24. Comparison of single blade C_T between μ=0.3 and fitted pitch curves. (a) [0.3,0.1]-fitted, (b) [0.4,0.1]-fitted and (c) [0.5,0.1]-fitted

Fig 25 shows the comparison of VAWT's C_P for different fitted pitch strategies and compared with μ=0.3. After fitting the *dpsf* pitch curves, the fluctuations of [0.3,0.1]-fitted disappear, while the [0.4,0.1]-fitted and [0.5,0.1]-fitted have small fluctuations. The reason for the small fluctuations is that [0.5,0.1] has the largest break distance at 180° azimuth, which resulted in the largest change in pitch angular velocity. Therefore, the worst fit is obtained from [0.5,0.1] when the same number of weight functions are used, so that more weight functions are needed to fit the curve. In subsequent studies, more suitable weight functions and number of weight coefficients are explored, and this paper demonstrates that continuity of pitch angular velocity is important for a suitable pitch strategy. The average C_P of different fitted pitch strategies is calculated and shown in Table 10. The C_P for [0.4,0.1]-fitted increased by 61.8% compared to those without the pitch and by 7.6% compared to μ = 0.3. The results show that this *dpsf* pitch strategy has better pitch effect than the single μ。

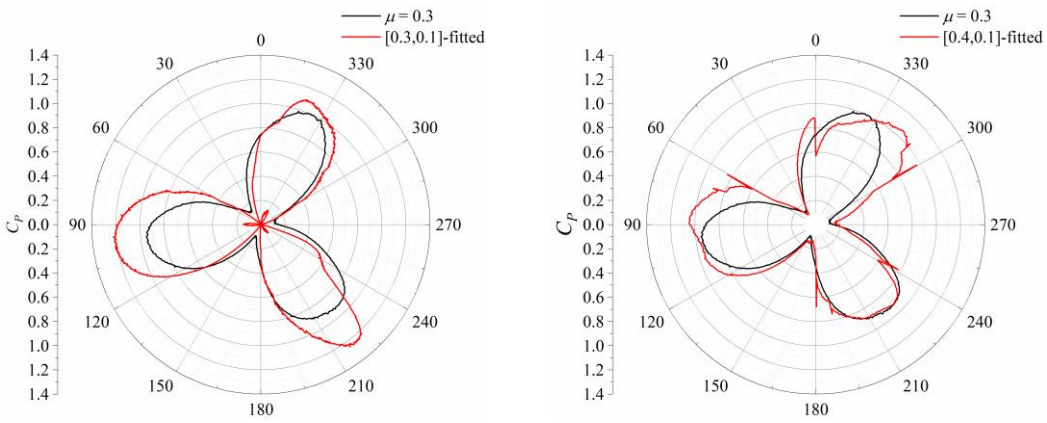

(a) (b)

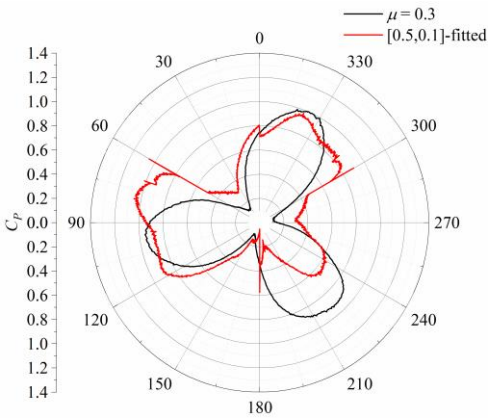

(c)

Fig. 25. Comparison of C_P of VAWT for μ=0.3 and fitted pitch strategies. Where the fitted pitch strategy in (a) is [0.3, 0.1]-fitted, (b) is [0.4, 0.1]-fitted, and (c) is [0.5, 0.1]-fitted.

539 Table 10 Results of C_P and growth rates for different fitted pitch strategies

	C_P	Growth rate/%
without pitch	34.9%	/
μ =0.3	53.8%	54.2%
[0.3, 0.1]-fitted	54.7%	56.7%
[0.4, 0.1]- fitted	56.5%	61.8%
[0.5, 0.1]- fitted	53.4%	53..0%

540 ## 6. Conclusion

541 In the paper, a pitch control strategy with azimuth variation is proposed based on the theoretical
542 AoA curve of VAWT. The AoA is proportionally changed at different azimuth angles by introducing
543 a pitch scale factor μ. For the small VAWT, the aim is to reduce the AoA significantly at azimuths
544 with larger AoA, although the AoA hardly changes at azimuths with small AoA. The different effects
545 of μ on the windward and leeward regions are analyzed. The conclusions of this work are
546 summarized as follows:
547
548 1. The pitch angle calculation equation was established. By applying a single pitch scale factor,
549 the C_P of VAWT increases by 146% and 54.2% at λ = 1.25 and λ = 1.5, respectively, when μ =
550 0.3. The pitch suppresses the generation of separation vortices at the leading edge of the airfoil
551 while avoiding the development of larger scale and stronger separation vortices at the trailing
552 edge. This greatly improves the aerodynamic performance of the VAWT.
553 2. When a single pitch scale factor is used, μ=0.5, -0.2 obtains the maximum C_P in the windward
554 and leeward regions, respectively. When a dual pitch scale factor is used, the best C_T curve
555 under the control of a single pitch scale factor cannot be obtained in both regions at the same
556 time. This is characterized by the fact that if the C_T in the leeward region is improved, the C_T in
557 the windward region is reduced and vice versa.
558 3. The pitch curves of sinusoidal-type pitch and pitch strategy in this paper are compared for the
559 same amplitude. The mean C_T of sinusoidal-type pitch is already lower than the baseline VAWT
560 for μ=0.3, and sinusoidal-type pitch makes the mean C_T equal to 0 for μ=0.5. However, the

application of the novel pitch strategy makes the C_T consistently higher than the baseline VAWT.

4. When using the dual pitch scale factor, the C_T curve generates large fluctuations at 0° (360°) and 180°. The reason for this occurrence is that there are two peaks points in the pitch angle curve, which lead to a discontinuity in the pitch angular velocity curve for these azimuths with large breaks. And the larger the breaking distance, the larger the fluctuation.
5. The pitch angle fitting curves with dual pitch scale factors are obtained and validated by fitting a weight function to the break distances, which effectively reduces the fluctuation amplitude. The pitch angle is locally corrected at $180°<\theta<210°$ and $300°<\theta<360°$. The results show that the C_P of the fitted curve is improved by 7.6% compared to a single pitch scaling factor and 61.8% over the baseline VAWT.

VAWTs, especially the small size one, are often used in urban areas. Pitch could turn the large scale wake vortices into fine and small vortices. This paper focuses on the influence of a novel pitch on the aerodynamic performance of the VAWT. Some further works are recommended for future studies in areas such as analyzing the effect of blade pitch on aerodynamic noise. In addition, this study mainly analyzed the effect of the novel pitch on the VAWT model at low tip speed ratio. The relationship between the aerodynamic performance and the pitch scale factor at high tip speed ratios can be further explored.

Authorship contribution statement

Qiang Zhang: Conceptualization, Methodology, Investigation, Software, Validation, Data curation, Writing – original draft. **Musa Bashir**: Conceptualization, Formal analysis, Writing - review & editing. **Weipao Miao**: Investigation, Resources, Data curation, Supervision, Funding acquisition. **Qingsong Liu**: Investigation, Resources, Data curation, Supervision, Funding acquisition. **Chun Li**: Investigation, Supervision, Funding acquisition, Project administration. **Minnan Yue**: Methodology, Conceptualization, Formal analysis. **Peilin Wang**: Investigation, Software, Validation.

Declaration of Competing Interest

The authors declare that they have no known competing financial interests or personal relationships that could have appeared to influence the work reported in this paper.

Acknowledgments

The authors would like to acknowledge the support of National Natural Science Foundation of China (grand No. 52006148, 52106262 and 51976131).

Reference

[1] Miao W, Liu Q, Xu Z, et al. A comprehensive analysis of blade tip for vertical axis wind turbine: Aerodynamics and the tip loss effect[J]. Energy Conversion and Management, 2022, 253: 115140.

[2] Atlaschian O, Metzger M. Numerical model of vertical axis wind turbine performance in realistic gusty wind conditions[J]. Renewable Energy, 2021, 165: 211-223.

[3] Liu Q, Miao W, Ye Q, et al. Performance assessment of an innovative Gurney flap for straight-bladed vertical axis wind turbine[J]. Renewable Energy, 2022, 185: 1124-1138.

[4] Tjiu W, Marnoto T, Mat S, et al. Darrieus vertical axis wind turbine for power generation I: Assessment of Darrieus VAWT configurations[J]. Renewable energy, 2015, 75: 50-67.

[5] Tescione G, Ragni D, He C, et al. Near wake flow analysis of a vertical axis wind turbine by stereoscopic particle image velocimetry[J]. Renewable Energy, 2014, 70: 47-61.

[6] Tjiu W, Marnoto T, Mat S, et al. Darrieus vertical axis wind turbine for power generation II: Challenges in HAWT and the opportunity of multi-megawatt Darrieus VAWT development[J]. Renewable Energy, 2015, 75: 560-571.

[7] Shankar P N. On the aerodynamic performance of a class of vertical shaft windmills[J]. Proceedings of the Royal Society of London. A. Mathematical and Physical Sciences, 1976, 349(1656): 35-51.

[8] WANG Z Y, ZHUANG M. Leading-edge serrations for performance improvement on a vertical-axis wind turbine at low tip-speed-ratios[J]. Applied energy, 2017, 208, 1184-1197.

[9] Ma N, Lei H, Han Z, et al. Airfoil optimization to improve power performance of a high-solidity vertical axis wind turbine at a moderate tip speed ratio[J]. Energy, 2018, 150: 236-252.

[10] CHEN J, LIN P, XU H, et al. A detail investigation of a novel vertical axis Darrieus wind rotor with two sets of blades[J]. Journal of Renewable and Sustainable Energy, 2017, 0133071.

[11] Maeda T, Kamada Y, Murata J, et al. Effect of solidity on aerodynamic forces around straight-bladed vertical axis wind turbine by wind tunnel experiments (depending on number of blades)[J]. Renewable energy, 2016, 96: 928-939.

[12] Minetto R A L, Paraschivoiu M. Simulation based analysis of morphing blades applied to a vertical axis wind turbine[J]. Energy, 2020, 202: 117705.

[13] Rockel S, Peinke J, Hölling M, et al. Wake to wake interaction of floating wind turbine models in free pitch motion: An eddy viscosity and mixing length approach[J]. Renewable Energy, 2016, 85: 666-676.

[14] Abbaszadeh S, Hoerner S, Maître T, et al. Experimental investigation of an optimised pitch control for a vertical-axis turbine[J]. IET Renewable Power Generation, 2019, 13(16): 3106-3112.

[15] Sharifi A, Nobari M R H. Prediction of optimum section pitch angle distribution along wind turbine blades[J]. Energy conversion and management, 2013, 67: 342-350.

[16] Sagharichi A, Zamani M, Ghasemi A. Effect of solidity on the performance of variable-pitch vertical axis wind turbine[J]. Energy, 2018, 161: 753-775.

[17] El-Fahham I, Abdelshahid G, Mokhiamar O. Pitch Angle Modulation of the Horizontal and Vertical Axes Wind Turbine Using Fuzzy Logic Control[J]. Processes, 2021, 9(8): 1337.

[18] Bayati I, Foletti S, Tarsitano D, et al. A reference open data vertical axis wind turbine, with individual pitch control, for code validation purposes[J]. Renewable Energy, 2018, 115: 711-720.

[19] Kosaku T, Sano M, Nakatani K. Optimum pitch control for variable-pitch vertical-axis wind turbines by a single stage model on the momentum theory[C]//IEEE International Conference on Systems, Man and Cybernetics. IEEE, 2002, 5: 6.

[20] Sheng Q, Khalid S S, Xiong Z, et al. CFD simulation of fixed and variable pitch vertical axis tidal turbine[J]. Journal of Marine Science and Application, 2013, 12(2): 185-192.

[21] Chen W, Zhou C Y. Application of numercal simulation to obtain the optimization pitch angle for VAWT[C]//2009 World Non-Grid-Connected Wind Power and Energy Conference. IEEE, 2009: 1-5.

[22] Bianchini A, Ferrara G, Ferrari L. Pitch optimization in small-size darrieus wind turbines[J]. Energy procedia, 2015, 81: 122-132.

[23] Thumthae C, Chitsomboon T. Optimal angle of attack for untwisted blade wind turbine[J]. Renewable energy, 2009, 34(5): 1279-1284.

[24] Chen Y, Kuang L, Su J, et al. Investigation of pitch angles on the aerodynamics of twin-VAWT under staggered arrangement[J]. Ocean Engineering, 2022, 254: 111385.

[25] Mazarbhuiya H M S M, Biswas A, Sharma K K. Low wind speed aerodynamics of asymmetric blade H-Darrieus wind turbine-its desired blade pitch for performance improvement in the built environment[J]. Journal of the Brazilian Society of Mechanical Sciences and Engineering, 2020, 42(6): 1-16.

[26] Ardaneh F, Abdolahifar A, Karimian S M H. Numerical analysis of the pitch angle effect on the performance improvement and flow characteristics of the 3-PB Darrieus vertical axis wind turbine[J]. Energy, 2022, 239: 122339.

[27] MacPhee D, Beyene A. Fluid-structure interaction of a morphing symmetrical wind turbine blade subjected to variable load[J]. International Journal of Energy Research, 2013, 37(1): 69-79.

[28] Maeda T, Kamada Y, Murata J, et al. Study on power performance for straight-bladed vertical axis wind turbine by field and wind tunnel test[J]. Renewable Energy, 2016, 90: 291-300.

[29] Huang M, Sciacchitano A, Ferreira C. On the wake deflection of vertical axis wind turbines by pitched blades[J]. Wind Energy, 2023, 26(4): 365-387.

[30] Bos R. Self-starting of a small urban Darrieus rotor. Strategies to boost performance in low-reynolds-number flows[D]. TU Delft University, 2012.

[31] Rathore M K, Agrawal M, Baredar P. Pitch Control Mechanism in Various Type of Vertical Axis Wind Turbines: A Review[J]. Journal of Vibration Engineering & Technologies, 2021: 1-17.

[32] Guo Y, Li X, Sun L, et al. Aerodynamic analysis of a step adjustment method for blade pitch of a VAWT[J]. Journal of Wind Engineering and Industrial Aerodynamics, 2019, 188: 90-101.

[33] Abdalrahman G, Melek W, Lien F S. Pitch angle control for a small-scale Darrieus vertical axis wind turbine with straight blades (H-Type VAWT)[J]. Renewable energy, 2017, 114: 1353-1362.

[34] LeBlanc B, Ferreira C. Estimation of blade loads for a variable pitch Vertical Axis Wind Turbine with strain gage measurements[J]. Wind energy, 2022, 25(6): 1030-1045.

[35] LeBlanc B, Ferreira C. Estimation of blade loads for a variable pitch vertical axis wind turbine from particle image velocimetry[J]. Wind Energy, 2022, 25(2): 313-332.

[36] Schönborn A, Chantzidakis M. Development of a hydraulic control mechanism for cyclic pitch marine current turbines[J]. Renewable energy, 2007, 32(4): 662-679.

[37] Paraschivoiu I, Trifu O, Saeed F. H-Darrieus wind turbine with blade pitch control[J]. International Journal of Rotating Machinery, 2009, 2009.

[38] Jain P, Abhishek A. Performance prediction and fundamental understanding of small vertical axis wind turbine with variable amplitude blade pitching[J]. Renewable Energy, 2016, 97: 97-113.

[39] Zhao Z, Qian S, Shen W, et al. Study on variable pitch strategy in H-type wind turbine considering effect of small angle of attack[J]. Journal of renewable and sustainable energy, 2017, 9(5): 053302.

[40] Li C, Xiao Y, Xu Y, et al. Optimization of blade pitch in H-rotor vertical axis wind turbines through computational fluid dynamics simulations[J]. Applied Energy, 2018, 212: 1107-1125.

[41] Chen L, Yang Y, Gao Y, et al. A novel real-time feedback pitch angle control system for vertical-axis wind turbines[J]. Journal of Wind Engineering and Industrial Aerodynamics, 2019, 195: 104023.

[42] Guevara P, Rochester P, Vijayaraghavan K. Optimization of active blade pitching of a vertical axis wind turbine

using analytical and CFD based metamodel[J]. Journal of Renewable and Sustainable Energy, 2021, 13(2): 023305.

[43] Zhang L, Gu J, Zhu H, et al. Rationality research of the adjustment law for the blade pitch angle of H-type vertical-axis wind turbines[J]. Renewable Energy, 2021, 167: 484-496.

[44] Rezaeiha A, Kalkman I, Blocken B. Effect of pitch angle on power performance and aerodynamics of a vertical axis wind turbine[J]. Applied energy, 2017, 197: 132-150.

[45] Bundi J M, Ban X, Wekesa D W, et al. Pitch control of small H-type Darrieus vertical axis wind turbines using advanced gain scheduling techniques[J]. Renewable Energy, 2020, 161: 756-765.

[46] Tsai H C, Colonius T. Coriolis effect on dynamic stall in a vertical axis wind turbine[J]. AIAA Journal, 2016, 54(1): 216-226.

[47] Brunner C E, Kiefer J, Hultmark M. Comparison of dynamic stall on an airfoil undergoing sinusoidal and VAWT-shaped pitch motions[C]//Journal of Physics: Conference Series. IOP Publishing, 2022, 2265(3): 032006.

[48] Hand B, Kelly G, Cashman A. Numerical simulation of a vertical axis wind turbine airfoil experiencing dynamic stall at high Reynolds numbers[J]. Computers & Fluids, 2017, 149: 12-30.

[49] Zhang L, Miao J, Gu J, et al. A method of reducing the radial load of the shaft of a vertical axis wind turbine based on movable mass blocks[J]. Renewable Energy, 2021, 175: 952-964.

[50] Hand B, Kelly G, Cashman A. Aerodynamic design and performance parameters of a lift-type vertical axis wind turbine: A comprehensive review[J]. Renewable and Sustainable Energy Reviews, 2021, 139: 110699.

[51] Tjiu W, Marnoto T, Mat S, et al. Darrieus vertical axis wind turbine for power generation I: Assessment of Darrieus VAWT configurations[J]. Renewable energy, 2015, 75: 50-67.

[52] Paraschivoiu I. Wind turbine design: with emphasis on Darrieus concept[M]. Presses inter Polytechnique, 2002.

[53] Liu Q, Miao W, Li C, et al. Effects of trailing-edge movable flap on aerodynamic performance and noise characteristics of VAWT[J]. Energy, 2019, 189: 116271.

[54] Manfrida G, Talluri L. Smart pro-active pitch adjustment for VAWT blades: Potential for performance improvement[J]. Renewable Energy, 2020, 152: 867-875.

[55] Elkhoury M, Kiwata T, Aoun E. Experimental and numerical investigation of a three-dimensional vertical-axis wind turbine with variable-pitch[J]. Journal of wind engineering and Industrial aerodynamics, 2015, 139: 111-123.

[56] Bianchini A, Balduzzi F, Bachant P, et al. Effectiveness of two-dimensional CFD simulations for Darrieus VAWTs: a combined numerical and experimental assessment[J]. Energy Conversion and Management, 2017, 136: 318-328.

[57] Menter F R. Two-equation eddy-viscosity turbulence modeling for engineering applications. AIAA Journal, 1994, 32(8), 1598-1605.

[58] Daroczy L, Janiga G, Petrasch K, Webner M, Thévenin D. Comparative analysis of turbulence models for the aerodynamic simulation of H-Darrieus rotors. Energy, 2015, 90: 680-690.

[59] Belamadi R, Djemili A, Ilinca A, et al. Aerodynamic performance analysis of slotted airfoils for application to wind turbine blades[J]. Journal of wind engineering and industrial aerodynamics, 2016, 151: 79-99.

[60] Ma N, Lei H, Han Z L, Zhou D, Bao Y, Zhang K, Zhou L, Chen C Y. Airfoil optimization to improve power performance of a high-solidity vertical axis wind turbine at a moderate tip speed ratio. Energy, 2018, 150: 236-252.

[61] Orlandi A, Collu M, Zanforlin S, et al. 3D URANS analysis of a vertical axis wind turbine in skewed flows[J]. Journal of Wind Engineering and Industrial Aerodynamics, 2015, 147: 77-84.

[62] Belabes B, Paraschivoiu M. Numerical study of the effect of turbulence intensity on VAWT performance[J]. Energy, 2021, 233: 121139.

[63] Siddiqui M S, Durrani N, Akhtar I. Quantification of the effects of geometric approximations on the performance of a vertical axis wind turbine[J]. Renewable Energy, 2015, 74: 661-670.